

RESEARCH ARTICLE

10.1002/2016JD025937

Key Points:

- CALIPSO data demonstrated good performance in estimating PBLH, and WCT appears to be a suitable technique
- CALIPSO results best agree with MPL and RS for winter and fall when aerosol loading is relatively high
- Elevated aerosol layers in spring and low aerosol loadings in summer are likely causes for the bias in CALIPSO PBLH

Supporting Information:

- Supporting Information S1

Correspondence to:

J. Li,
jing-li@pku.edu.cn

Citation:

Su, T., J. Li, C. Li, P. Xiang, A. K.-H. Lau, J. Guo, D. Yang, and Y. Miao (2017), An intercomparison of long-term planetary boundary layer heights retrieved from CALIPSO, ground-based lidar, and radiosonde measurements over Hong Kong, *J. Geophys. Res. Atmos.*, 122, 3929–3943, doi:10.1002/2016JD025937.

Received 17 SEP 2016

Accepted 8 MAR 2017

Accepted article online 13 MAR 2017

Published online 4 APR 2017

An intercomparison of long-term planetary boundary layer heights retrieved from CALIPSO, ground-based lidar, and radiosonde measurements over Hong Kong

Tianning Su¹ , Jing Li² , Chengcai Li² , Pengzhan Xiang², Alexis Kai-Hon Lau³, Jianping Guo⁴ , Dongwei Yang², and Yucong Miao⁴

¹Department of Atmospheric and Oceanic Sciences, University of Maryland, College Park, Maryland, USA, ²Department of Atmospheric and Oceanic Sciences, Peking University, Beijing, China, ³Department of Civil and Environmental Engineering and Institute for the Environment, Hong Kong University of Science and Technology, Kowloon, Hong Kong, ⁴State Key Laboratory of Severe Weather, Chinese Academy of Meteorological Sciences, Beijing, China

Abstract The planetary boundary layer height (PBLH) is a very important parameter in the atmosphere, because it determines the range where the most effective dispersion processes take place, and serves as a constraint on the vertical transport of heat, moisture, and pollutants. As the only space-borne lidar, Cloud-Aerosol Lidar with Orthogonal Polarization onboard Cloud-Aerosol Lidar and Infrared Pathfinder Satellite Observations (CALIPSO) measures the vertical distribution of aerosol signals and thus offers the potential to retrieve large-scale PBLH climatology. In this study, we explore different techniques for retrieving PBLH from CALIPSO measurements and validate the results against those obtained from ground-based micropulse lidar (MPL) and radiosonde (RS) data over Hong Kong, where long-term MPL and RS measurements are available. Two methods, namely maximum standard deviation (MSD) and wavelet covariance transform (WCT), are used to retrieve PBLH from CALIPSO. Results show that the RS- and MPL-derived PBLHs share similar interannual variation and seasonality and can complement each other. Both MSD and WCT perform reasonably well compared with MPL/RS products, especially under sufficient aerosol loading. Uncertainties increase when aerosol loading is low and the CALIPSO signal consequently becomes noisier. Overall, CALIPSO captures the general PBLH seasonal variability over Hong Kong, despite a high bias in spring and a low bias in summer. The spring high bias is likely associated with elevated aerosol layers due to transport, while the summer low bias can be attributed to higher noise level associated with weaker aerosol signal.

1. Introduction

The planetary boundary layer (PBL) is the lowest layer of the atmosphere. It exerts an essential impact on the surface-atmosphere exchanges of energy, moisture, momentum, heat, gases, and pollutants. The PBL is generally dominated by complicated, nonlinear, and chaotic turbulence, which leads to the relatively strong vertical mixing of gas, moisture, and aerosols. Therefore, the height of the PBL, named PBLH, determines the vertical extent to which the most effective dispersion process takes place and is a key parameter in weather and climate [Seibert *et al.*, 2000; Haefelin *et al.*, 2011], as well as pollution studies [Seinfeld and Pandis, 2006]. The PBLH is also a crucial length scale in atmospheric numerical models [Monks *et al.*, 2009; Gan *et al.*, 2011].

Traditional methods for deriving PBLH include gradient methods [e.g., Johnson *et al.*, 2001; Liu and Liang, 2010] and Richardson number methods [e.g., Vogelesang and Holtslag, 1996; Guo *et al.*, 2016], both of which are based on profiles of temperature, pressure, humidity, and wind speed obtained by radiosondes (RS). However, using RS to retrieve PBLH bears several shortcomings. On one hand, RS are often launched at nonoptimal times for determining PBLH. According to the policy of World Meteorological Organization, regular RS in China are routinely launched twice daily at 0800 and 2000 China Standard Time (CST), when PBLH is not fully developed. On the other hand, the spatial coverage of RS sites is usually too sparse to capture PBLH spatial variability. Apart from RS, ground-based lidar, such as micropulse lidar (MPL), which measures extinction by aerosols, has also been widely used to derive PBLH [e.g., Hägeli *et al.*, 2000; He *et al.*, 2008; Tucker *et al.*, 2009; Yang *et al.*, 2013]. The lidar algorithm is based on the fact that a temperature inversion often exists at the top of PBL that traps moisture and aerosols [Seibert *et al.*, 2000], which leads to a sharp decrease in aerosol backscatter signals at the upper boundary of the PBL. Therefore, the location of the PBL upper boundary can be determined by finding the steepest gradient of aerosol backscattering signals.

Lidar-derived PBLHs generally show good coherence with RS products [e.g., Cooper and Eichinger, 1994; Hennemuth and Lammert, 2006; Sawyer and Li, 2013]. However, as a ground-based method, it still suffers from poor spatial coverage.

As the only space-borne lidar in operation, the Cloud-Aerosol Lidar with Orthogonal Polarization (CALIOP) onboard Cloud-Aerosol Lidar and Infrared Pathfinder Satellite Observations (CALIPSO) [Winker et al., 2007] has the capability of retrieving vertical distributions of clouds and aerosols with high vertical resolution and offers a great potential for the estimation of global PBLHs from space. Based on the idea that there is a local maximum in the vertical standard deviation of lidar backscatter at the PBL top [Melfi et al., 1985], Jordan et al. [2010] determined the PBLH from CALIPSO as the lowest occurrence of a local maximum in the standard deviation of backscatter profile collocated with a maximum in the backscatter itself. McGrath-Spangler and Denning [2012] modified this method by restricting the retrieved depths to 0.25–5 km, adding a check for surface noise, and removing profiles with attenuating and overlying clouds. Several studies further proved the effectiveness of CALIPSO data by presenting overall reasonable agreements between CALIPSO-derived and RS-based/MPL-based PBLH results [e.g., Leventidou et al., 2013; Liu et al., 2015; Zhang et al., 2016].

Although previous studies produced promising results from CALIPSO, there are still some limitations that should be noticed. A major difficulty in using CALIPSO to derive PBLH compared to ground-based methods is its low signal-to-noise ratio (SNR). In particular, because of the long travel distance of attenuated backscatter, the signals reaching the CALIPSO lidar from low altitudes can be much noisier compared with ground-based lidar [Winker et al., 2007; Mamouri et al., 2009]. This increases the difficulty in determining the precise height of the PBL top. Another problem is that previous studies utilizing CALIPSO data were typically based on maximum standard deviation (MSD) method [e.g., Jordan et al., 2010; McGrath-Spangler and Denning, 2012; Liu et al., 2015], whereas another widely used method, the wavelet covariance transform (WCT), has been largely ignored. WCT is an effective tool introduced by Gamage and Hagelberg [1993] in distinguishing the step changes from noisy signals. It has demonstrated good performance in PBLH estimation from MPL [e.g., Davis et al., 2000; Brooks, 2003; Compton et al., 2013] and other ground-based measurements. However, there is still lack of discussion about the application of the WCT technique to CALIPSO data.

Based on the above-mentioned shortcomings, this study attempts to provide the first comparison and evaluation of CALIPSO-derived PBLH using both MSD and WCT techniques. Several refinements have been made to the WCT method to better account for cloud screening, surface detection, noisy signals, etc. Moreover, we also present a comprehensive assessment of the results using 7 years of PBLHs derived from RS and MPL. We focus our study on the Hong Kong area since a unique long-term MPL record is available here, which allows for the evaluation of both the accuracy and seasonal variability of the CALIPSO results. To our knowledge, this is the first long-term, detailed intercomparison between RS-, MPL-, and CALIPSO-derived PBLH products. We further examine the differences between CALIPSO and MPL/RS for different seasons and under different aerosol loadings and discuss possible sources of uncertainties.

The paper proceeds as follows: Section 2 introduces the methods for retrieving PBLH from CALIPSO as well as from RS and MPL. The detailed intercomparison results between RS-, MPL-, and CALIPSO-derived PBLHs, including their seasonal variation and bias, are presented in section 3. A brief conclusion is given in section 4.

2. Data and Method

2.1. Site Description

We use CALIPSO, MPL, and RS to calculate PBLHs over Hong Kong, a megacity located at the Pearl River Delta of China. Hong Kong is one of the most densely populated and well-urbanized regions in the world. The climate of this region is dominated by the southerly/southwesterly East Asia monsoon in summer and northerly/northeasterly monsoon in winter [Yuan et al., 2013].

In the Hong Kong area, there are three MPL stations operated by the Hong Kong University of Science and Technology (HKUST): Yuelong (YL, 22°26'N, 114°1'E), Sha Tau Kok (STK, 22°32'N, 114°12'E), and HKUST Pump House (PH, 22°20'N, 114°16'E). The RS station (22°10'N, 114°19'E) operated by the Hong Kong Observatory routinely launches RS at 0800 and 2000 CST every day. Figure 1 shows the location of YL (blue

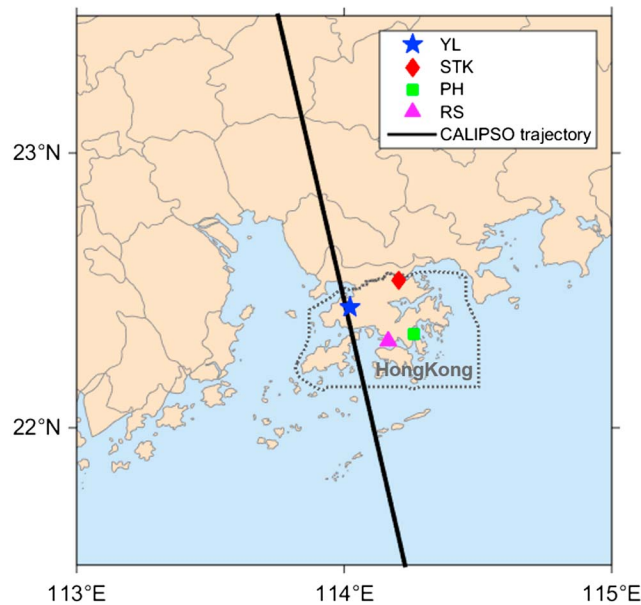


Figure 1. Geographic distributions of the three MPL sites: YL, STK, and PH. The RS station is also shown in pink triangle, with CALIPSO orbit track superimposed (black line).

star), STK (red rhombus), PH (green square), and RS (pink triangle) stations, with the daytime CALIPSO orbit tracks (black line) near Hong Kong superimposed. The daytime CALIPSO orbits overpassing Hong Kong is very close to the three MPL sites (less than 10 km from YL station and ~30 km from STK and PH station, cf. Figure 1), which creates a favorable condition for the comparison against ground-based observations. For matching up between CALIPSO and MPL retrievals, we select the nearest position in CALIPSO orbit to the MPL station and then average the available CALIPSO retrievals within 20 km around this position.

2.2. Retrieving PBLHs From CALIPSO

As part of the Afternoon satellites constellation (A-train) [L'Ecuyer and

Jiang, 2010], CALIPSO is in a 705 km Sun-synchronous polar orbit between 82°N and 82°S with a 16 day repeat cycle and with equator crossings at approximately 1330 and 0130 local time [Winker et al., 2007; Winker et al., 2009]. CALIOP aboard the CALIPSO platform is the first space-borne lidar optimized for aerosol and cloud profiling, which has the 532 nm channel (parallel and perpendicular polarization) and the 1064 nm channel. CALIOP measures total attenuated backscatter coefficient (TAB) with a horizontal resolution of 1/3 km and vertical resolution of 30 m in the low and middle troposphere. The attenuated backscatter data (Level 1B) is publicly available online from the Atmospheric Science Data Center at NASA Langley Research Center (<https://www.nasa.gov/langley>). Because the nighttime heavy surface inversion and residual layers complicate the identification of the PBL, we only focus on daytime observations for this analysis.

In this study, we utilized the MSD method developed by McGrath-Spangler and Denning [2012] and adopt the threshold method initially proposed by Platt et al. [1994] to identify clouds using the threshold value indicated by Okamoto et al. [2007]. Although under some circumstances the top height of boundary layer clouds can be regarded as the PBLH, such estimation requires the correct identification of cloud type which cannot be accurately determined by the lidar. Therefore, the cloudy conditions have been subsequently excluded from the following analysis. We also made several additional modifications and refinements. First of all, the restricted altitude has been modified to the range of 0.3 to 2.5 km according to the characteristics of PBLH over Hong Kong. Moreover, because CALIPSO views from above, when penetrating through an aerosol layer, the signals often become attenuated when it reaches the bottom of the layer. This generates a decline in TAB below the top of the aerosol layer which may also result in a local maximum of TAB standard deviation. However, this local maximum is not created by the natural jump of aerosol concentration from the PBL to the free atmosphere, but rather by the viewing geometry of the instrument. To address this issue, we define a function:

$$\beta(i) = \max\{f(i + 2), f(i + 1)\} - \min\{f(i), f(i - 1)\} \tag{1}$$

where $f(i + 2)$, $f(i + 1)$, $f(i)$, $f(i - 1)$ are four adjacent altitude bins of 532 nm TAB, with the attitude decreasing with increasing bin number i . We add a constraint of $\beta > 0$ for PBLH identification, which can eliminate the local maximum of standard deviation caused by signal attenuation at low altitudes and ensures that the location of the PBLH lies at the top of the aerosol layer.

To better illustrate this treatment, Figure 2a shows an example of PBLH results derived from CALIPSO using the MSD technique. The TAB from CALIPSO on 24 October 2007 over Hong Kong is plotted with a horizontal

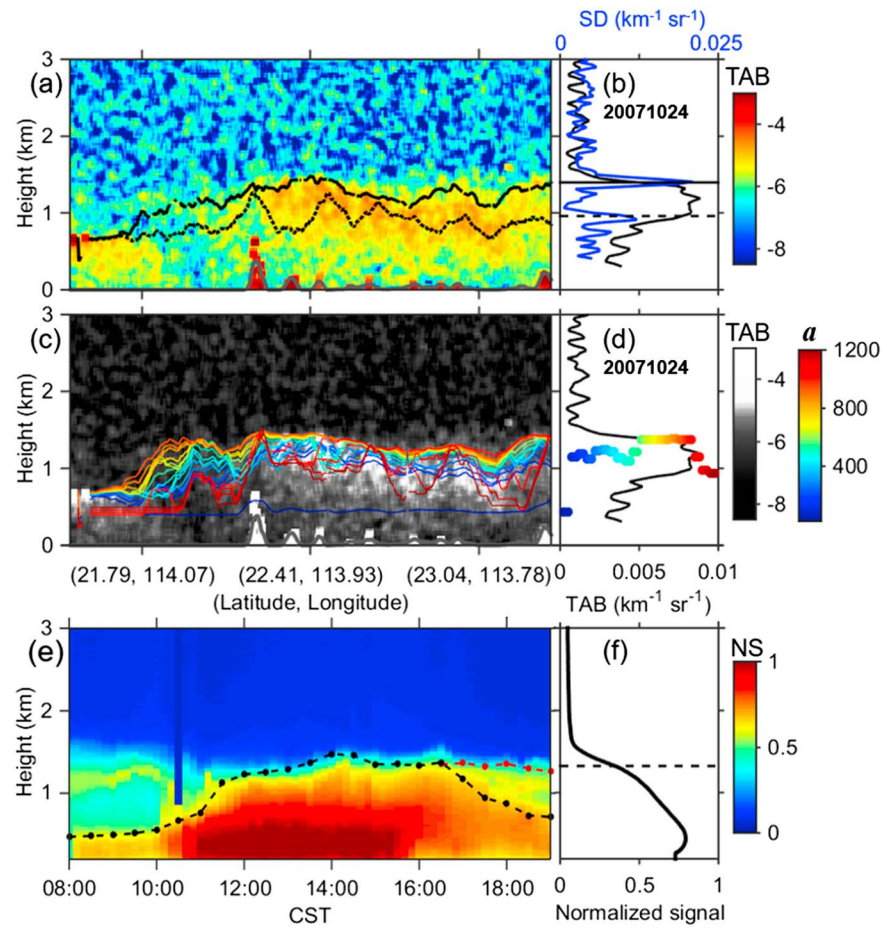


Figure 2. (a) Total attenuated backscatter (TAB) plot (log scale) from CALIPSO on 24 October 2007 over Hong Kong. The black lines indicate the derived PBLH using MSD method with constraint $\beta > 0$ (solid) and without constraint (dashed). The gray line represents surface elevation. (b) The vertical profile of TAB (black curve) and the vertical standard deviation (blue curve) of TAB closest to the MPL site. (c) and (d) Similar to Figures 2a and 2b, except that the lines and dots indicate the derived PBLH using the WCT method. The curves in different colors represent various PBLHs based on the assumption of various dilation a values used in wavelet covariance transform method. The midpoints of Figures 2a and 2c are the positions closest to MPL. (e) Time evolution of the NS plot from MPL on 24 October 2007. The black line identifies the PBLH derived from MPL, and the red line represents the residual layer. (f) The NS profile of MPL averaged from 1300 to 1400 CST.

smoothing of 3 km and a vertical sliding window of 90 m to improve the SNR. The solid black line indicates the derived PBLH using MSD method with constraint $\beta > 0$ and the dashed line shows that without constraint. A horizontal smoothing of 7 km is applied to the retrieved PBLHs in order to minimize the influence of outliers and to increase its spatial consistency. Figure 2b presents the vertical profiles of TAB (black) and the vertical standard deviation (blue) of TAB close to the MPL site (YL) averaged over 20 km. We can see that there are two local maxima in the standard deviation profile. The lower one is caused by the signal attenuation by the aerosols above, which is effectively eliminated by the constraint of $\beta > 0$. Hereafter, the method using MSD technique with constraint is simply referred to as “MSD.”

In addition, we also introduce the WCT technique to derive PBLH from the TAB profiles of CALIPSO. We use a Haar wavelet whose function h is defined as [Gamage and Hagelberg, 1993]:

$$h\left(\frac{z-b}{a}\right) = \begin{cases} +1 : & b - \frac{a}{2} \leq z \leq b \\ -1 : & b < z \leq b + \frac{a}{2} \\ 0 : & \text{elsewhere} \end{cases} \quad (2)$$

where z is altitude, b is called the “translation” of the function where the function is centered, and a is called

the “dilation” of the function. Then, the covariance transform of the Haar function $W_f(a, b)$ is defined as follows:

$$W_f(a, b) = \frac{1}{a} \int_{z_b}^{z_t} f(z) h\left(\frac{z-b}{a}\right) dz \quad (3)$$

where $f(z)$ is the backscatter signal of the lidar, z_b is the lower limit and z_t is the higher limit of the profile. The value b at which $W_f(a, b)$ reaches the local maximum with a coherent scale of a is usually considered as the PBLH. The selection of dilation a is the key in this processes. Brooks [2003] proposed that the best selection of dilation a should equal the transition zone range of the ideal profile. In previous studies, the selection of dilation a generally ranges from 100 m to 1000 m for ground-based lidar [e.g., Davis *et al.*, 2000; Brooks, 2003; Compton *et al.*, 2013]. For choosing an appropriate dilation a suitable for the TAB profiles derived from CALIPSO, we perform a series of sensitivity tests. Figure 2c presents the derived PBLHs using WCT techniques with different a values roughly within the range of those used in previous studies. Figure 2d shows the corresponding results for a spatially averaged profile which is the same as Figure 2b. The specific $W_f(a, b)$ function corresponding to different values of the dilation a can be found in Figure S1 in the supporting information. The selected PBLH retrieval range, surface noise check, and cloud screening are the same as the MSD method. It is seen from Figure 2d that when the dilation a is chosen between 600 m to 900 m, the PBLH results show no substantial difference and all correctly identify the top of the aerosol layer. We therefore consider this range appropriate. Note that this range is larger than the typical value used for MPL [Brooks, 2003] since larger dilation is required to smooth out the noisier CALIPSO signals. We choose the dilation a as 690 m and make sure that there do not exist obvious unrealistic conditions through visual inspection. The method using WCT will be simply referred to as “WCT” in the following text.

2.3. Retrieving PBLHs From MPLs

The MPL located at the YL station is a SESI Model 1000 produced by the SESI Corporation and was continuously operated from June 2006 to December 2009. This MPL stopped working due to facility malfunction since January 2010 and was replaced by MPL-4B produced by Sigma Space since October 2011. The other two MPLs located at STK and PH stations, respectively, are both Sigma Space MPL-4B model. The basic information for these MPLs is presented in Table 1. Background subtraction, saturation, afterpulse, overlap, and range corrections are applied to raw MPL data to derive the normalized signal (NS) with arbitrary units.

For retrieving PBLH from MPL measurements, we follow a well-established method, which was developed by Flamant *et al.* [1997] and then refined by Yang *et al.* [2013]. It retrieves daytime PBLH based on the criterion of signal gradient minimum, namely the signal gradient reaching minimum at the top of the PBL. The first derivative of a Gaussian filter is first applied to smooth the vertical profile of NS and to produce the gradient profile. Multiple valleys and peaks of gradient profile are identified, representing the stratification structure of aerosol. The first significant peak of the gradient profile is regarded as the upper limit for searching PBL top, and then the deepest valley of the gradient profile is identified as PBLH. For cloud screening, we use the same threshold method by Platt *et al.* [1994] and eliminate false results caused by clouds. A manual quality assurance to correctly identify the PBLH is implemented due to the following possible contaminations: (1) When the PBL is not fully identified, the algorithm tends to identify the top of residual layers as the PBLH; (2) occasionally, there can be more than one significant decrease in the signal profile. The one that is the most consistent with retrieval results at the previous time step is selected to ensure temporal consistency of the daytime PBLH. More detailed description about manual quality assurance can be found in Yang *et al.* [2013]. Nonetheless, only a small fraction of the data (5%) is eliminated by the manual quality assurance.

To collocate with CALIPSO overpass, we use PBLH retrievals averaged from 1300 to 1400 CST, when the PBL is well developed, with its depth generally reaching daily maximum. This is referred to as “noontime PBLHs.” As an example, Figure 2e shows the temporal evolution of the NS from MPL on 24 October 2007. The black line indicates the PBLH derived from MPL, and the red line represents the residual layer. During this day, CALIPSO-derived PBLHs using the two methods agreed well with those derived from MPL. The noontime PBLH is around 1.3 km in this case.

2.4. Retrieving PBLH From RS

To partly resolve the problem that RS cannot provide continuous daily PBLH products, we turn to the method proposed by Holzworth [1964, 1967] to produce diurnally varying PBLH using morning potential temperature

Table 1. Description of MPLs at Different Stations

Station	Observed Period	Lidar Type	Temporal Resolution (s)	Vertical Resolution (m)	Wavelength (nm)
YL	Jun 2006–Dec 2009	SESI Model 1000	15	30	523.5
	Oct 2011–Jun 2013	Sigma Space MPL-4B	10	7.5	532
STK	Oct 2007–May 2010	Sigma Space MPL-4B	10	7.5	532
PH	Jan 2011–Jun 2013	Sigma Space MPL-4B	15	15	532

profile and daily surface potential temperature. The Holzworth method is a very useful tool to estimate PBLH and has been widely used by a range of studies [e.g., Du *et al.*, 2013; Zhang *et al.*, 2014; Lai, 2015; Karimian *et al.*, 2016]. Briefly, along with the increase of surface temperature from the morning, this method assumes that the air mass is lifted adiabatically from the surface to higher altitudes and maintains a nearly constant potential temperature. The height at which the environment potential temperature and current surface potential temperature reaches equilibrium is estimated to be the upper boundary of the PBL. Conventionally, the environment potential temperature profile is measured by the radiosonde launched at 0800 CST at the RS station (shown in Figure 1), and the diurnal trend of surface potential temperature is determined by the hourly surface potential temperatures obtained from the meteorological facilities at the YL station. The Holzworth method assumes that the potential temperature remains constant for the same day at the same altitude of the free atmosphere and also assumes that the potential temperature is homogenous within the PBL. However, note that due to the more complicated real conditions, the PBLH estimated from these ideal assumptions cannot be regarded as “truth” and thus we use it jointly with MPL for validating CALIPSO results.

3. Results and Discussion

3.1. An Overview of RS-Derived and MPL-Derived PBLHs Over Hong Kong

By utilizing the algorithm described above, we obtain a long-term PBLH data set from RS and MPL measurements over Hong Kong during the period from June 2006 to June 2013. The MPL results at the YL station overlap with Yang *et al.* [2013] from June 2006 to December 2009, while the rest of the data set is originally presented by this study. Figure 3a shows the time series of noontime PBLHs derived from RS and MPL at YL, STK, and PH sites, respectively, from June 2006 to June 2013, smoothed with a 70 day sliding window. The PBLHs retrieved from MPLs and RS exhibit similar seasonal variation and interannual variability, both capturing the temporal characteristics of PBLHs over Hong Kong. In general, annual PBLH reaches maximum in late summer/early fall and becomes the lowest in winter. There also appears to be a slight decreasing trend from 2006 to 2013, although its significance and cause need further investigation. Figure 3b shows the time span of each data set with the total number of noontime retrievals indicated on the right y axis. The gap in the YL time series is caused by instrument maintenance and facility malfunction and is partly filled by STK and PH data. During the study period, there are 148 times when CALIPSO overpasses Hong Kong following the orbit shown in Figure 1.

Figure 4 further compares MPL- and RS-retrieved PBLH for all three stations jointly and each station individually. For precise comparison, the RS results in Figure 4 is produced by considering the difference in the variability of potential temperature within the PBL at different MPL sites and using the hourly variation of surface potential temperature at each site along with the potential temperature profile obtained by RS. We can see that the two methods yield very consistent results, with the correlation coefficients (R) well above 0.6 for most cases. This result verifies the reliability of both types of ground-based PBLH estimates, which will be later used to validate CALIPSO results.

3.2. Comparison Between PBLHs Derived From CALIPSO and MPL/RS

In this section, we compare and evaluate in detail CALIPSO-derived PBLH against RS and MPL results, as well as between the MSD and WCT methods.

Figure 5 shows the scatter plots of CALIPSO-derived PBLH by the two approaches against those obtained from the MPL at YL (Figure 5b), STK (Figure 5c), PH (Figure 5d), and all these three stations (Figure 5a). The PBLHs derived from MPL and RS are again averaged between 1300 to 1400 CST. Figure 5 indicates that CALIPSO-derived PBLH using MSD and WCT both agree well with MPL. The correlation coefficients are

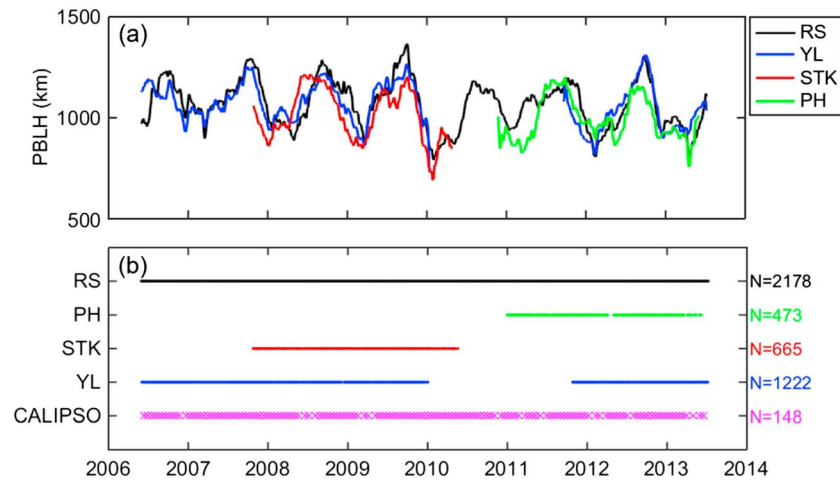


Figure 3. (a) Time series of noontime mean PBLHs derived from RS and MPLs at YL, STK, and PH, respectively, from June 2006 to June 2013. A 70 day sliding window has been applied to each line. (b) The available noontime validated PBLH sampling numbers retrieved from RS and MPLs of YL, STK, and PH, respectively. The pink crosses refer to the overpass times of CALIPSO.

mostly above 0.6 and reach the highest value (~0.7) at YL. The root-mean-square error (RMSE) between WCT and MPL is lower than that for MSD, which well indicates that the WCT technique can be quite suitable for retrieving PBLH from CALIPSO data and even outperforms MSD. Compared with MPL versus RS, CALIPSO PBLHs bear larger differences from RS results (Figure 5e), with both lower correlation and higher RMSE. This phenomenon is in part due to the different standards used to estimate PBLH for these two types of

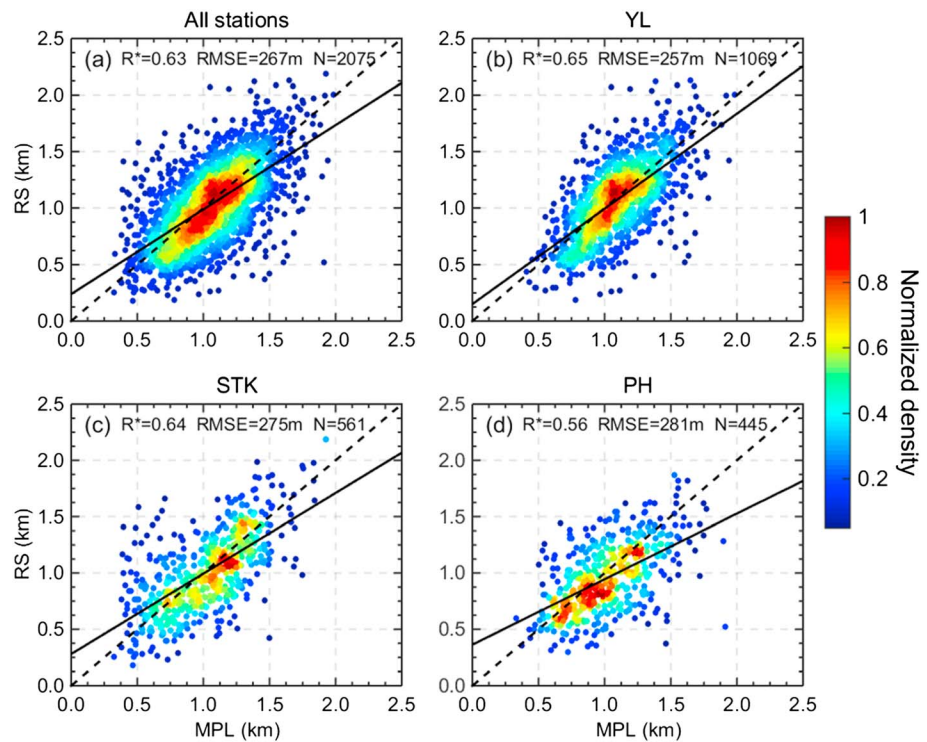


Figure 4. The comparison of noontime PBLHs derived from MPL and RS at (a) all the three stations, (b) YL, (c) STK, and (d) PH. The color-shaded dots indicate the normalized sample density. The correlation coefficients (R), RMSE, and sample numbers (N) are given in each panel. Here and in the following analysis, the superscript star of R indicates that the confidence level is above 99%.

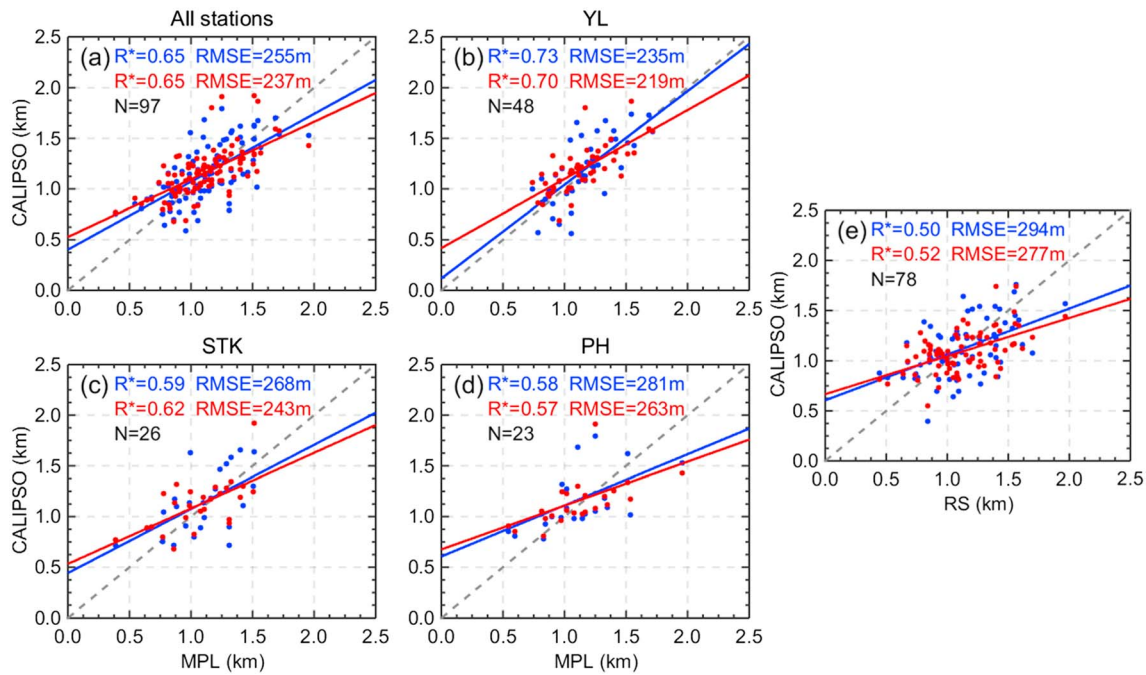


Figure 5. The comparison of noontime PBLHs derived from CALIPSO and MPL at (a) all the three stations, (b) YL, (c) STK, and (d) PH. (e) The comparison of noontime PBLHs derived from CALIPSO and RS. The blue lines and dots are derived from MSD, while the red lines and dots are derived from WCT.

measurements: both CALIPSO and MPL retrievals are based on aerosol concentration, whereas RS retrieval is based on thermodynamic condition.

A detailed examination between MSD and WCT is given in Figure 6. The two methods yield very consistent results, with a high correlation ($R=0.83$ in Figure 6a). From the distribution of the differences shown in Figure 6b, a slightly high bias is noticed for WCT. The difference between the two approaches and MPL are mostly confined within ± 0.4 km (Figures 6c–6d), with an averaged absolute difference of 0.2 km for MSD and 0.19 km for WCT. CALIPSO results are slightly biased high compared to MPL. The difference between CALIPSO and RS is larger (Figures 6e–6f), with average absolute differences of 0.26 km and 0.24 km, respectively.

3.3. Comparison of PBLH Climatology

The climatology of PBLH, especially its seasonal variability, is also very important in climate and air pollution related studies. Figure 7 shows distributions of noontime PBLHs over Hong Kong from MPLs, RS, and CALIPSO (using both MSD and WCT) for spring (MAM), summer (JJA), autumn (SON), and winter (DJF). For MPL, we mainly use the products obtained at the YL station, with the gap between January 2010 to September 2011 partly filled by STK and PH data. Overall, the PBLH over Hong Kong exhibits a clear seasonal cycle, with maximum in autumn and minimum in winter, consistent with Figure 3 and previous study by Yang *et al.* [2013]. RS- and MPL-derived PBLHs agree well in terms of seasonality, only with a slightly larger range of variability for RS. CALIPSO also captures general PBLH seasonal variability for both approaches. We note that the average value of CALIPSO-derived PBLHs agree well with MPL and RS in the fall and winter, whereas larger differences are found in spring and summer.

Compared to CALIPSO, MPL and RS also have the advantage of capturing diurnal PBLH variability. Figure 8 further shows the monthly averaged diurnal cycle of PBLH derived from MPL and RS, with CALIPSO results overlaid at approximately 1330 CST. The MPL-derived and RS-derived PBLHs show similar characteristics of diurnal cycle; i.e., it grows rapidly from 0800 CST, reaches maximum around 1400 CST, maintains a relatively high value until 1600 CST, and then starts to drop. The daily maximum PBLH typically increases from January, achieving a maximum of around 1.2 km in October, and then rapidly declining to 0.93 km in December. Figure 8 also confirms that the largest disagreements in monthly averaged results between CALIPSO and

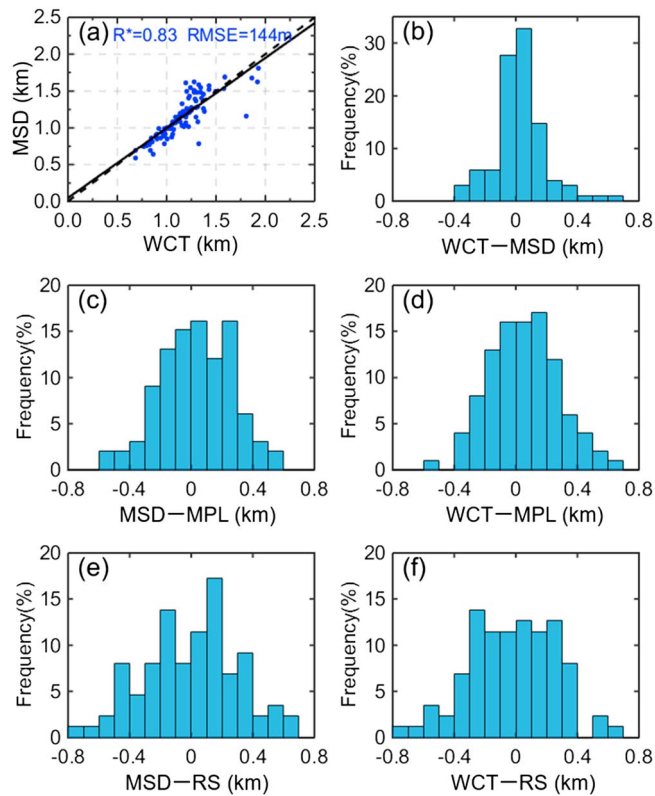


Figure 6. (a) The comparison of CALIPSO-derived PBLH between MSD method and WCT method. (b)–(f) Histogram of PBLH differences: (b) MSD versus WCT, (c) MSD versus MPL, (d) WCT versus MPL, (e) MSD versus RS, and (f) WCT versus RS.

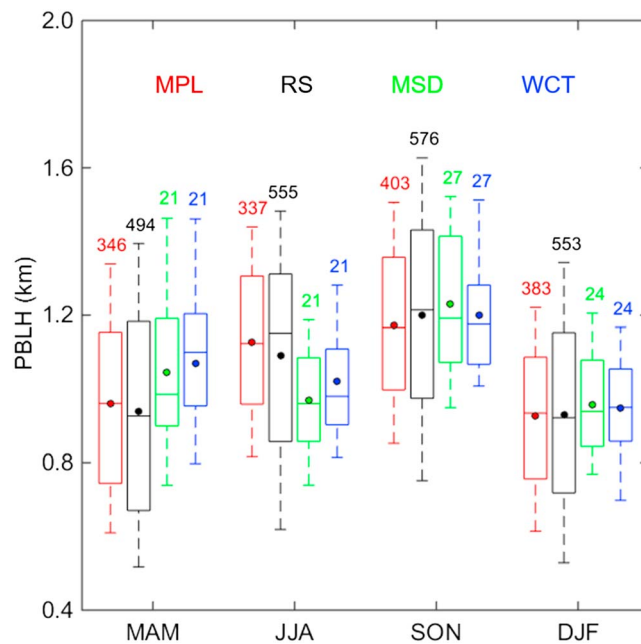


Figure 7. Seasonal box-and-whisker plots showing 10th, 25th, 50th, 75th, and 90th percentile values of PBLH derived from MPL (red), RS (black), MSD (green), and WCT (blue) for MAM (spring), JJA (summer), SON (autumn), and DJF (winter), respectively. The dots indicate the mean PBLH for each method. The numbers above each box refer to the number of samples.

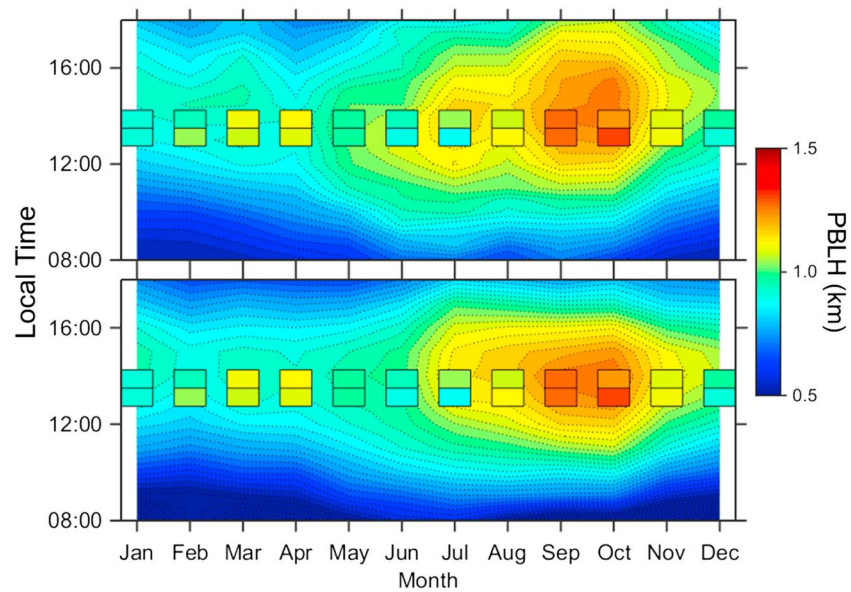


Figure 8. (a) Monthly mean diurnal variation of PBLH derived from MPL. (b) Monthly mean diurnal variation of PBLH derived from RS. The squares represent the monthly mean PBLHs derived from two approaches of CALIPSO at approximately 1330 CST. The lower rectangles indicate MSD results, while the upper ones indicate WCT results.

MPL/RS are in the spring and summer. In particular, an overestimate as large as 0.2 km is found for March and April while an underestimate of similar magnitude is observed during June and July.

3.4. Seasonal Biases and Its Causes

As noted above, a seasonal disagreement is found in PBLH climatology. Here we continue to explore the possible causes for these seasonal biases. The seasonally averaged absolute differences between different methods (calculated from matched cases of noontime PBLHs) are presented in Figure 9a. To reduce station bias, only the YL station is used for the analysis. Similar to the climatology pattern, we also found that the absolute differences between CALIPSO and MPL/RS are the highest in spring and summer. Because the retrieval of PBLH from CALIPSO depends on aerosol backscatter signal, we further separately examine the absolute difference under different aerosol loadings, namely clear, moderate, and polluted conditions (Figure 9b). The different conditions are classified using PM_{10} measurements made at the YL station (see Figure S3). A distinct contrast can be seen in Figure 9b, with clear condition corresponding to the highest mean absolute differences while the polluted condition bears the lowest mean absolute differences. This phenomenon is particularly obvious for the averaged absolute differences between CALIPSO and MPL, which reach 0.24 km for clean conditions but fall to 0.14 km for polluted conditions.

The change of CALIPSO error with aerosol loading is likely associated with its signal to noise ratio. Because the detection of PBL top purely depends on the contrast between aerosol signal and clear sky signal, a cleaner sky reduces this contrast and makes it less discernable from noise. To better illustrate this, Figure 10 compares PBLH retrieval between a clean case ($PM_{10} = 26 \mu\text{g}/\text{m}^3$, cf. Figures 10a and 10b) and a polluted case ($PM_{10} = 108 \mu\text{g}/\text{m}^3$, cf. Figures 10c and 10d). For the clear condition, the aerosol layer is obscured by noise without an identifiable upper boundary of the PBL in CALIPSO TAB. Therefore, both MSD and WCT tend to locate the PBLHs at the local gradient maximum caused by the noise, which is below the actual PBLH identified by MPL (marked as stars in Figure 10). By contrast, for the polluted condition, the SNR becomes much higher, and the sharp gradient of aerosol backscatter at the top of the PBL can be well identified by the two algorithms. Typically, aerosol loading is the lowest in the summer for Hong Kong, (see Figure S4), which tends to increase the uncertainty of CALIPSO retrievals.

In the spring, it is a different story. As indicated by previous work, Hong Kong may suffer from pollution transported from mainland China during this season [He *et al.*, 2008]. In our analysis, we do notice many cases of elevated aerosol layers in both MPL and CALIPSO images in the spring, which is separated from PBL aerosols.

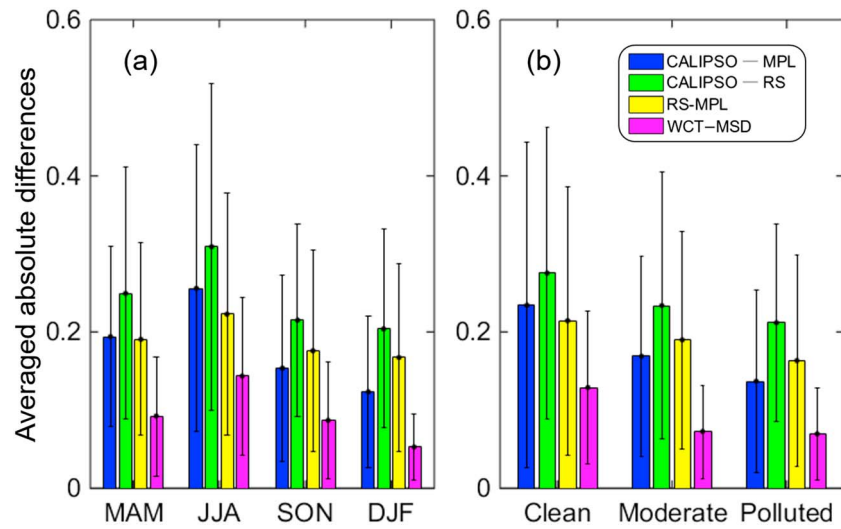


Figure 9. The averaged absolute bias of noontime PBLHs between different methods (a) for MAM, JJA, SON, and DJF, respectively, and (b) for clean, moderate, and polluted conditions, respectively. The error bars represent their standard deviations.

As the CALIPSO laser travels from above, its intensity often becomes much weaker after passing this elevated layer and thus cannot well observe the PBL signals below. Therefore, in these cases, the upper boundary of the elevated aerosol layer tends to be misclassified as PBL top.

Figure 11 presents a typical case of multiple aerosol layer structure. From the MPL image (Figure 11a), there is an elevated layer with large backscatter signal from 1.5 to 2 km. The NS and depolarization ratio profile

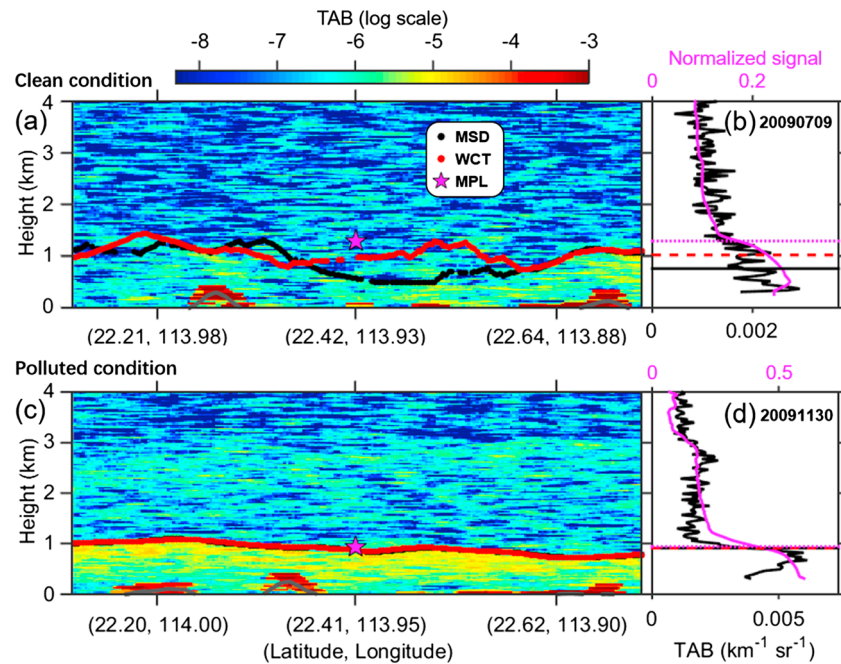


Figure 10. (a) TAB plot from CALIPSO on 9 July 2009 (clean) and (c) 30 November 2009 (polluted). The black lines indicate the derived PBLH using MSD method, and the red lines indicate that derived using WCT method. The gray lines represent the surface. The pink stars indicate the PBLH derived from MPL, and the midpoints of Figures 10a and 10c are the positions closest to MPL. In Figures 10b and 10d, the black curves indicate the corresponding vertical profile of TAB derived from CALIPSO profile closest to the MPL site, while the pink lines indicate the MPL NS profile averaged from 1300 to 1400. The horizontal black, red, and pink lines indicate the PBLH derived from MSD, WCT, and MPL, respectively.

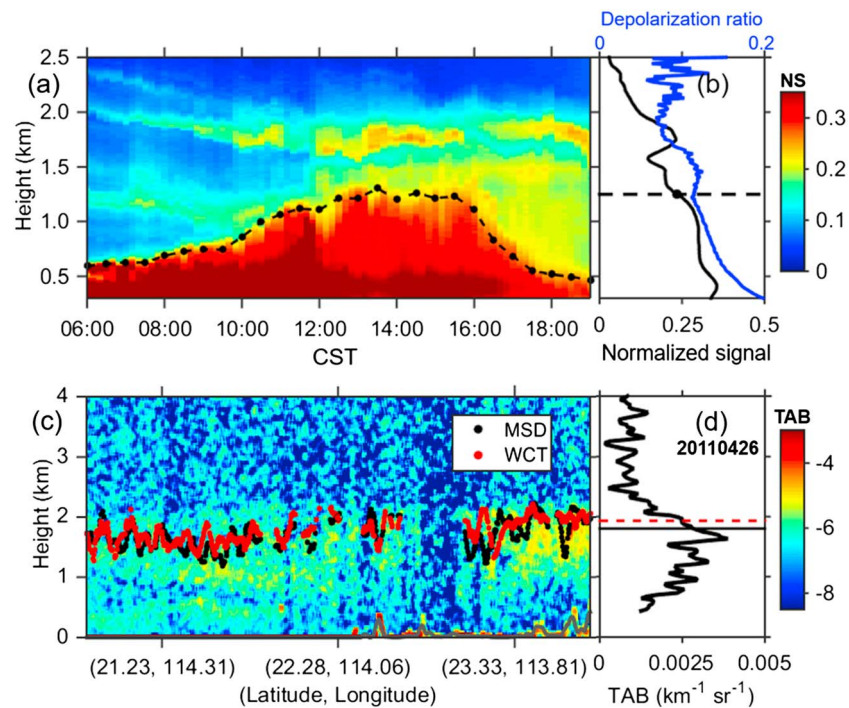


Figure 11. (a) Time evolution of the NS plot from MPL on 26 April 2011. The black line identifies the PBLH derived from MPL. (b) The NS and depolarization profiles derived from MPL average from 1300 to 1400 CST. (c) TAB plot from CALIPSO on 26 April 2011. The black lines indicate the derived PBLH using MSD method, while the red lines indicate that derived using WCT method. The gray lines represent the surface. The midpoint of Figure 11c is the position closest to MPL. (d) The black curve indicates the corresponding vertical profile of TAB derived from CALIPSO closest to the MPL site. The horizontal black and red lines indicate the PBLH derived from MSD and WCT, respectively.

averaged over 1300 to 1400 is presented in Figure 11b. The relatively low corresponding depolarization ratio suggests that the upper layer may be fine pollution particles transported from inland, while the PBL may be dominated by pollutants mixed with large sea-salt particles which have higher depolarization ratios. Figure 11c shows the corresponding TAB plot from CALIPSO on 26 April 2011. From the CALIPSO image, however, no clear two-layer structure can be identified. As discussed above, when the CALIPSO laser beam traverses the elevated aerosol layer (1.6 km to 2 km), the signal is already attenuated, and thus, the lower aerosol layer cannot be fully detected. As a result, both MSD and WCT tend to locate the PBLH as the top of upper aerosol layer. Since elevated aerosol layers occur most frequently in the spring (Figure S4), they are likely responsible for CALIPSO's high spring bias.

3.5. Comparison Between the Two Approaches

From the above comparisons, we noticed that while PBLH retrievals using the two techniques are mostly consistent, some differences still exist. As already shown in Figure 9 (magenta bars), the differences between the two methods are mostly below 0.1 km, with the largest difference in summer and the smallest in winter. Their differences are also closely related to aerosol loading (Figure 9b). Clear condition corresponds to the highest mean absolute differences (0.13 km) between the two methods, while the polluted condition corresponds to the lowest mean absolute differences (0.07 km). This analysis further indicates that seasonal characteristics of pollution levels can affect the consistency and thus the uncertainty level between the two approaches.

Comparing these two methods, the implementation of MSD is comparatively simple, making it a widely used method in retrieving PBLHs from CALIPSO data [e.g., Jordan *et al.*, 2010; McGrath-Spangler and Denning, 2012; McGrath-Spangler and Denning, 2013; Liu *et al.*, 2015]. Nonetheless, the local maximum in the standard deviation of the backscatter profile is not always located at the PBL top, because of signal attenuation and random noises of backscatter. On the other hand, WCT is less subject to random noise and usually achieve better results under low SNR conditions, yet it is a scale-dependent approach involving the choice of the

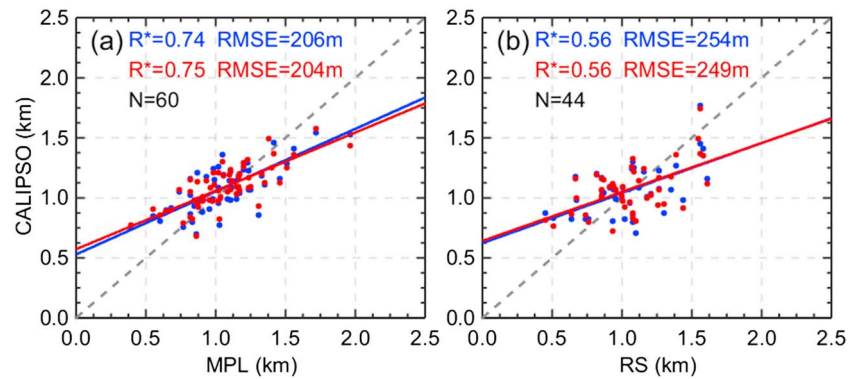


Figure 12. (a) The updated correlation of PBLH derived from CALIPSO and MPL after eliminating cases when the difference between MSD and WCT is above 100 m. (b) The same as Figure 12a but for the comparison between CALIPSO and RS.

wavelet function and a few other parameters. However, our study shows that WCT can be effective in retrieving PBLHs from CALIPSO with an appropriate selection of dilation a .

Finally, by eliminating cases when the difference between MSD and WCT is above 100 m, the agreement between CALIPSO and MPL/RS results is much improved (Figure 12). Thus, jointly using two methods can produce more reliable results. Nonetheless, this is still partly related to aerosol loading since when the two methods are more consistent, aerosol loading is usually high, and thus, the agreement between CALIPSO and MPL/RS also becomes better.

4. Conclusions

In this study, we explore the applicability of two techniques: MSD and WCT, to the retrieval of PBLH using CALIPSO backscatter profiles. Results are validated against 7 years of ground-based MPL and RS measurements over Hong Kong. Both the accuracy and seasonal variability of CALIPSO PBLH are examined in detail, and possible sources of uncertainty are investigated.

Overall, CALIPSO PBLH compares reasonably well with both MPL and RS. WCT performs slightly better than MSD with a lower overall RMSE. Distinct seasonal characteristics are also observed in PBLH over Hong Kong. PBLH reaches the highest value in the fall and decreases in winter and early spring. CALIPSO largely captures this seasonality, albeit with a high bias in spring and low bias in summer. Moreover, we originally identify two conditions, namely low aerosol loading and elevated aerosol layer, that are mainly the reason for the bias in CALIPSO retrievals. Specifically, detailed examination indicates that the summer low bias is likely associated with low SNR caused by insufficient aerosol loading, while the spring high bias can be attributed to elevated aerosol layers (pollutants transported from inland). Insufficient aerosol loading also appears to be the main reason for the disagreement found between MSD and WCT results. It also should be noted that the biases caused by low aerosol loading and elevated aerosol layers are mostly caused by the problem of signal quality and are thus difficult to be fundamentally solved by the improvement of algorithms. Another related issue to note is that for cases when aerosols are not fully mixed within the entire PBL, the height identified by our algorithms (or any algorithm based on aerosol concentration) will be the height of the mixed layer, which is not necessarily the same as the PBLH. Nonetheless, this issue is not significant in the cases examined in this study.

While previous studies mostly focused on the MSD method, our results show that WCT technique with appropriate choice of parameters is well applicable for CALIPSO data and can even outperform MSD, which provides the basis of using this methodology to retrieve PBLH from CALIPSO. This technique provides a scale-dependent approach while retaining all of the information in the original backscatter profile and is useful for detecting steps through noisy signal. Another novelty of our study is the introduction of constraint parameter β , which successfully avoids the misclassification of the PBLH as the bottom of the signal-strong aerosol layer. Moreover, by using the two methods jointly, there is potential for even better estimates, as cases with better agreement between the two methods are also found to be more consistent with MPL and RS.

For further studies, we plan to extend the current work to a larger spatial scale. The major advantage of satellite observations is its extensive spatial coverage, which makes it possible to more comprehensively examine the variability of PBLH in space and time. Such large-scale PBLH climatology will be valuable for weather forecast, climate change, and air pollution research.

Acknowledgments

We thank the CALIPSO team for providing the CALIPSO Level 1B data used for this study. This data set is downloaded from <https://eosweb.larc.nasa.gov/project/calipso/>. We also thank the Environmental Central Facility at the Institute for the Environment, Hong Kong University of Science and Technology for providing the radiosonde data (data link: <http://envf.ust.hk/dataview/lidar/current/>). The RS data are provided by the data center of China Meteorological Administration (CMA, <http://data.cma.cn/data/index/e6ba725cabfd8fb.html>). This work is funded by National Science Foundation of China (NSFC) grants 41375008, 41575018, and 91544217.

References

- Brooks, I. M. (2003), Finding boundary layer top: Application of a wavelet covariance transform to lidar backscatter profiles, *J. Atmos. Oceanic Technol.*, *20*(8), 1092–1105.
- Compton, J. C., R. Delgado, T. A. Berkoff, and R. M. Hoff (2013), Determination of planetary boundary layer height on short spatial and temporal scales: A demonstration of the covariance wavelet transform in ground-based wind profiler and lidar measurements, *J. Atmos. Oceanic Technol.*, *30*(7), 1566–1575.
- Cooper, D. I., and W. E. Eichinger (1994), Structure of the atmosphere in an urban planetary boundary layer from lidar and radiosonde observations, *J. Geophys. Res.*, *99*(D11), 22,937–22,948, doi:10.1029/94JD01944.
- Davis, K. J., N. Gamage, C. R. Hagelberg, C. Kiemle, D. H. Lenschow, and P. P. Sullivan (2000), An objective method for deriving atmospheric structure from airborne lidar observations, *J. Atmos. Oceanic Technol.*, *17*(11), 1455–1468.
- Du, C., S. Liu, X. Yu, X. Li, C. Chen, Y. Peng, Y. Dong, Z. Dong, and F. Wang (2013), Urban boundary layer height characteristics and relationship with particulate matter mass concentrations in Xi'an, central China, *Aerosol Air Qual. Res.*, *13*, 1598–1607.
- Flamant, C., J. Pelon, and P. Flamant (1997), Lidar determination of the entrainment zone thickness at the top of the unstable marine atmospheric boundary layer, *Boundary Layer Meteorol.*, *83*(2), 247–284.
- Gamage, N., C. Hagelberg (1993), Detection and analysis of microfronts and associated coherent events using localized transforms, *J. Atmos. Sci.*, *50*, 750–756.
- Gan, C.-M., Y. Wu, B. Madhavan, B. Gross, and F. Moshary (2011), Application of active optical sensors to probe the vertical structure of the urban boundary layer and assess anomalies in air quality model PM_{2.5} forecasts, *Atmos. Environ.*, *45*(37), 6613–6621, doi:10.1016/j.atmosenv.2011.09.013.
- Guo, J., et al. (2016), The climatology of planetary boundary layer height in China derived from radiosonde and reanalysis data, *Atmos. Chem. Phys.*, *16*(20), 13,309–13,319.
- Haefelin, M., et al. (2011), Evaluation of mixing-height retrievals from automatic profiling lidars and ceilometers in view of future integrated networks in Europe, *Boundary Layer Meteorol.*, *143*(1), 49–75, doi:10.1007/s10546-011-9643-z.
- Hägeli, P., D. Steyn, and K. Strawbridge (2000), Spatial and temporal variability of mixed-layer depth and entrainment zone thickness, *Boundary Layer Meteorol.*, *97*(1), 47–71.
- He, Q., C. Li, J. Mao, A. K.-H. Lau, and D. A. Chu (2008), Analysis of aerosol vertical distribution and variability in Hong Kong, *J. Geophys. Res.*, *113*, D14211, doi:10.1029/2008JD009778.
- Hennemuth, B., and A. Lammert (2006), Determination of the atmospheric boundary layer height from radiosonde and lidar backscatter, *Boundary Layer Meteorol.*, *120*(1), 181–200, doi:10.1007/s10546-005-9035-3.
- Holzworth, G. (1964), Estimates of mean maximum mixing depths in the contiguous United States, *Mon. Weather Rev.*, *92*(5), 235–242.
- Holzworth, G. (1967), Mixing depths, wind speeds and air pollution potential for selected locations in the United States, *J. Appl. Meteorol.*, *6*(6), 1039–1044.
- Johnson, R. H., P. E. Ciesielski, and J. A. Cotturone (2001), Multiscale variability of the atmospheric mixed layer over the western Pacific warm pool, *J. Atmos. Sci.*, *58*, 2729–2750.
- Jordan, N. S., R. M. Hoff, and J. T. Bacmeister (2010), Validation of Goddard Earth Observing System-version 5 MERRA planetary boundary layer heights using CALIPSO, *J. Geophys. Res.*, *115*, D24218, doi:10.1029/2009JD013777.
- Karimian, H., Q. Li, C. Li, L. Jin, J. Fan, and Y. Li (2016), An improved method for monitoring fine particulate matter mass concentrations via satellite remote sensing, *Aerosol Air Qual. Res.*, *16*(4), 1081–1092.
- Lai, L. W. (2015), Fine particulate matter events associated with synoptic weather patterns, long-range transport paths and mixing height in the Taipei Basin, Taiwan, *Atmos. Environ.*, *113*, 50–62.
- L'Ecuyer, T. S., and J. H. Jiang (2010), Touring the atmosphere aboard the A-Train, *Phys. Today*, *63*(7), 36–41.
- Leventidou, E., P. Zanis, D. Balis, E. Giannakaki, I. Pytharoulis, and V. Amiridis (2013), Factors affecting the comparisons of planetary boundary layer height retrievals from CALIPSO, ECMWF and radiosondes over Thessaloniki, Greece, *Atmos. Environ.*, *74*, 360–366.
- Liu, J., J. Huang, B. Chen, T. Zhou, H. Yan, H. Jin, Z. Huang, and B. Zhang (2015), Comparisons of PBL heights derived from CALIPSO and ECMWF reanalysis data over China, *J. Quant. Spectrosc. Radiat. Transfer*, *153*, 102–112.
- Liu, S., and X.-Z. Liang (2010), Observed diurnal cycle climatology of planetary boundary layer height, *J. Clim.*, *22*(21), 5790–5809, doi:10.1175/2010JCLI3552.1.
- Mamouri, R. E., V. Amiridis, A. Papayannis, E. Giannakaki, G. Tsaknakis, and D. S. Balis (2009), Validation of CALIPSO space-borne-derived attenuated backscatter coefficient profiles using a ground-based lidar in Athens, Greece, *Atmos. Meas. Tech.*, *2*(2), 513–522.
- McGrath-Spangler, E. L., and A. S. Denning (2012), Estimates of North American summertime planetary boundary layer depths derived from space-borne lidar, *J. Geophys. Res.*, *117*, D15101, doi:10.1029/2012JD017615.
- McGrath-Spangler, E. L., and A. S. Denning (2013), Global seasonal variations of midday planetary boundary layer depth from CALIPSO space-borne LIDAR, *J. Geophys. Res. Atmos.*, *118*, 1226–1233, doi:10.1002/jgrd.50198.
- Melfi, S. H., J. D. Spinhrine, S. H. Chou, and S. P. Palm (1985), Lidar observations of vertically organized convection in the planetary boundary layer over the ocean, *J. Clim. Appl. Meteorol.*, *24*(8), 806–821.
- Monks, P., et al. (2009), Atmospheric composition change global and regional air quality, *Atmos. Environ.*, *43*(33), 5268–5350, doi:10.1016/j.atmosenv.2009.08.021.
- Okamoto, H., et al. (2007), Vertical cloud structure observed from shipborne radar and lidar: Midlatitude case study during the MR01/K02 cruise of the research vessel Mirai, *J. Geophys. Res.*, *112*, D08216, doi:10.1029/2006JD007628.
- Platt, C. M., et al. (1994), The experimental cloud lidar pilot study (ECLIPS) for cloud-radiation research, *Bull. Am. Meteorol. Soc.*, *75*(9), 1635–1654.
- Sawyer, V., and Z. Li (2013), Detection, variations and intercomparison of the planetary boundary layer depth from radiosonde, lidar and infrared spectrometer, *Atmos. Environ.*, *79*, 518–528.
- Seibert, P., F. Beyrich, S.-E. Gryning, S. Joffre, A. Rasmussen, and P. Tercier (2000), Review and intercomparison of operational methods for the determination of the mixing height, *Atmos. Environ.*, *34*(7), 1001–1027, doi:10.1016/S1352-2310(99)00349-0.

- Seinfeld, J. H., and S. N. Pandis (2006), *Atmospheric Chemistry and Physics: From Air Pollution to Climate Change*, 2nd ed., John Wiley, Hoboken, N. J.
- Tucker, S. C., et al. (2009), Doppler lidar estimation of mixing height using turbulence, shear, and aerosol profiles, *J. Atmos. Oceanic Technol.*, *26*(4), 673–688.
- Vogelezang, D. H. P., and A. A. M. Holtslag (1996), Evaluation and model impacts of alternative boundary layer height formulations, *Boundary Layer Meteorol.*, *81*(3–4), 245–269, doi:10.1007/BF02430331.
- Winker, D. M., W. H. Hunt, and M. J. McGill (2007), Initial performance assessment of CALIOP, *Geophys. Res. Lett.*, *34*, L19803, doi:10.1029/2007GL030135.
- Winker, D. M., M. A. Vaughan, A. Omar, Y. Hu, K. A. Powell, Z. Liu, W. H. Hunt, and S. A. Young (2009), Overview of the CALIPSO mission and CALIOP data processing algorithms, *J. Atmos. Oceanic Technol.*, *26*, 2310–2323.
- Yang, D., C. Li, A. K. H. Lau, and Y. Li (2013), Long-term measurement of daytime atmospheric mixing layer height over Hong Kong, *J. Geophys. Res. Atmos.*, *118*, 2422–2433.
- Yuan, Z., V. Yadav, J. R. Turner, P. K. K. Louie, and A. K. H. Lau (2013), Long-term trends of ambient particulate matter emission source contributions and the accountability of control strategies in Hong Kong over 1998–2008, *Atmos. Environ.*, *76*, 21–31.
- Zhang, W., J. Guo, Y. Miao, H. Liu, Y. Zhang, Z. Li, and P. Zhai (2016), Planetary boundary layer height from CALIOP compared to radiosonde over China, *Atmos. Chem. Phys.*, *16*, 9951–9963, doi:10.5194/acp-16-9951-2016.
- Zhang, Y., Z. Gao, D. Li, Y. Li, N. Zhang, X. Zhao, and J. Chen (2014), On the computation of planetary boundary-layer height using the bulk Richardson number method, *Geosci. Model Dev.*, *7*(6), 2599–2611.